Development 134, 3437-3448 (2007) doi:10.1242/dev.007906

SOX3 activity during pharyngeal segmentation is required for craniofacial morphogenesis

Karine Rizzoti* and Robin Lovell-Badge

Craniofacial development is a complex multi-step process leading to the morphogenesis of the face and sense organs, and to that of the neck, including the anteriormost part of the respiratory and digestive apparatus and associated endocrine glands. In vertebrates, the process is initiated by the formation of the pharyngeal arches from ectoderm, endoderm and mesoderm. These arches are then populated by neural crest cells, which originate from the central nervous system. We show here that, in mouse, there is a requirement for the HMG box factor SOX3 during the earliest stage of pharyngeal development: the formation of the pharyngeal pouches that segment the pharyngeal region by individualising each arch. In *Sox3*-null mutants, these pouches are expanded at the detriment of the second pharyngeal arch. As a consequence, neural crest cell migration and ectoderm-derived epibranchial placode development are affected, leading to craniofacial defects. We also show that *Sox3* genetically interacts both with *FgfR1* and with *Sox2*, another member of the Soxb1 family, to fulfil its function in the pharyngeal region. Although the importance of the neural crest has long been recognised, our studies highlight the equally crucial role of the pharyngeal region in craniofacial morphogenesis. They also give insight into the formation of pharyngeal pouches, of which little is known in vertebrates. Finally, this work introduces two new players in craniofacial development – SOX3 and SOX2.

KEY WORDS: SOX HMG box factor, Conditional gene deletion, Craniofacial development, Pharyngeal segmentation, Mouse

INTRODUCTION

The formation of the pharyngeal arches (PA) relies on complex interactions between tissues of the three primary germ layers, ectoderm, endoderm, mesoderm, and also neural crest cells (ncc). They will later contribute elements of the face and the pharyngeal apparatus. In mammals, the first PA gives rise to the lower jaw, whereas the second forms the hyoid apparatus. The external and middle ear also develop from these two arches. Posteriorly the third and fourth arches participate in the formation of the throat (Graham and Smith, 2001). In humans, craniofacial dysmorphologies are common, ranging from simple facial disfigurement to conductive deafness, thyroid deficiency and more complex syndromes, such as DiGeorge (Wurdak et al., 2006).

In the mouse, ncc originating from the hindbrain begin to populate the PA at 8 days post-coitum (dpc). The cells stemming from rhombomeres (r) 1 and 2, then 4, and finally 6 and 7, migrate to the first, second and posterior PA respectively, where they surround mesodermal cells located at their core. A layer of ectoderm is present externally, whereas the internal surface of the arches is lined by endoderm. As morphogenesis takes place, ncc form skeletal and connective tissues. Mesodermal cells give rise to the muscles and endothelial cells of the arch arteries. The epidermis and sensory neurons of the epibranchial ganglia derive from the ectoderm, while the epithelium lining the pharynx and the pharyngeal endocrine glands (thymus, thyroid and parathyroids) develop from the endoderm.

The neural crest was thought to be the tissue mostly responsible for patterning the pharyngeal arches, but it has been shown that they still develop and are properly regionalised in its absence (Gavalas et al., 2001; Veitch et al., 1999). It is now clear that the endoderm is another important source of information for the formation of this region (Graham et al., 2004; Graham and Smith, 2001).

Development of the pharyngeal pouches (PP), a characteristic of all chordates, is the first physical manifestation of pharyngeal segmentation. By physically individualising each arch they also define their anteroposterior polarity. The PP initially develop at specific sites where the endoderm forms an outpocketing and engages in direct contact with overlying ectoderm; they then open and gradually elongate along the proximodistal axis of the arches (Quinlan et al., 2004). They are surrounded by a newly formed epithelium, the pouch margin. In mouse, *Fgf8* interacts genetically with *Tbx1*, implicated in DiGeorge syndrome (Jerome and Papaioannou, 2001), for correct pharyngeal patterning (Arnold et al., 2006; Vitelli et al., 2002) and a hypomorphic mutation of *Fgfr1* leads to agenesis of the proximal domain of PA2 at the benefit of the flanking pouches (Trokovic et al., 2003). In *Tbx1* mutant mice, fusion of the distal ganglia of the ninth (IX) and tenth (X) cranial nerves illustrates another important function of the PP endoderm: at early stages it induces overlying ectoderm to form the epibranchial placodes, which give rise to the distal portion of the cranial ganglia (Baker and Bronner-Fraser, 2001).

The X-linked gene *Sox3*, which encodes an HMG box protein, is predominantly expressed throughout the developing central nervous system (CNS), in a pattern similar to the two other members of the *SoxB1* subfamily, *Sox1* and *Sox2* (Collignon et al., 1996; Wood and Episkopou, 1999). Mice deleted for *Sox3* are affected by hypopituitarism (Rizzoti et al., 2004), as are human patients carrying *SOX3* mutations (Laumonnier et al., 2002), reflecting the important role of the protein in the CNS. The mutant mice, and a subset of the human patients, are also affected by craniofacial defects. We have now uncovered the origin of the latter phenotype, and our results are consistent with SOX3 being required within the pharyngeal epithelia for craniofacial morphogenesis to proceed normally.

Division of Developmental Genetics, MRC National Institute for Medical Research, The Ridgeway, Mill Hill, London NW7 1AA, UK.

*Author for correspondence (e-mail: krizzot@nimr.mrc.ac.uk)

Accepted 17 July 2007

MATERIALS AND METHODS

Mice

Sox3 (Rizzoti et al., 2004) and *Fgfr1*^{n7} (Trokovic et al., 2003) alleles were maintained respectively on MF1 and ICR outbred backgrounds. All mouse experiments used protocols approved under the UK Animal (scientific procedures) Act.

Skeletal preparations, in situ hybridisation, whole-mount immunofluorescence and phalloidin staining

Skeletal preparations (Trokovic et al., 2003) and whole-mount in situ hybridisation (Avilion et al., 2000) were performed as described. Probe references are available on request.

For whole-mount immunofluorescence, embryos were fixed for 2 hours in 4% PFA on ice. Antibodies were incubated overnight at 4°C: anti-CRABPI (Abcam) 1/250, 2H3 (Developmental Hybridoma Bank) 1/40 for neurofilament detection, anti-N-cadherin (Zymed) 1/200, anti-GFP (Molecular Probes) 1/500, anti-SOX2 (Chemicon) 1/500, anti-SOX3 (a gift from T. Edlund) 1/500 or (R&D Systems) 1/300, Alexa 594- and Alexa 488-conjugated secondary antibodies (Molecular Probes) 1/500 and HRP-conjugated anti-mouse antibody (Jackson laboratories) 1/300. Fluorescence-stained embryos were cleared as described (Zucker et al., 1999). Confocal images were obtained using a Leica TCS SP microscope and TCSNT software. Volocity software was used for 3D reconstructions. DAB-stained embryos were cleared in glycerol for whole-mount imaging or processed for histology.

Phalloidin-stained embryos were fixed overnight in 4% PFA, 0.2 μg/ml TRITC-conjugated phalloidin (Sigma), mounted in Vectashield (Molecular Probes) and analysed by confocal microscopy.

Apoptosis detection

After CRABPI immunofluorescence on frozen sections, apoptotic cells were detected using the ApopTag Fluorescein kit (Serologicals Corporation). Apoptotic cells within a restricted CRABPI positive domain were counted on three sections per embryo on both sides (n=7). Analysis of variance was performed comparing the number of apoptotic cells on each side, and significance was estimated using Student's t-test.

RESULTS

Sox3 deletion affects craniofacial development

Sox3$^{\Delta gfp}$ hemizygous XY or homozygous XX mice (*Sox3* null mutants) show variable phenotypes, characterised by hypopituitarism and craniofacial defects. Although CNS defects were found to be responsible for the hypopituitarism, both the nature and the origin of the latter phenotype were not investigated (Rizzoti et al., 2004). We have found malformation, displacement or, in extreme cases, absence of the pinna in 50% of hemizygous mutants (n=62). These malformations were asymmetric, exclusively affecting the left ear in 74.2% of cases. Tooth overgrowth due to jaw misalignment also affected 41.9% of the mutants, and asymmetric paralysis of the vibrissae was found in 17.7% (Fig. 1A,B).

To analyse these defects, skeletal preparations of newborn animals were examined (Fig. 1C-H). These revealed middle ear defects, but did not show any other obvious skeletal abnormalities (Fig. 1C,D), except for a reduction in ossification of facial bones in the null animals [compare the chondrocytic Alcian Blue staining between wild type (Fig. 1C,E,G) and *Sox3* null littermates (Fig. 1D,F,H)]. As pituitary hormones influence skeletal growth (Robson et al., 2002), it is possible that this deficit/delay is linked to their hypopituitarism.

Defects in the middle ear and surrounding elements (styloid process and hyoid bone) were variable and highly asymmetric, with the left side predominantly affected (Fig. 1I, n=14). The styloid process was most often affected (Fig. 1E,F,I) and, less frequently, the stapes and the lesser horns of the hyoid bone. The distal part of the malleus, comprising the manubrium and the processus brevis, could also be abnormal and, in one case, was found to be missing (Fig. 1E-I and data not shown). In extreme cases the tympanic ring was reduced or absent (Fig. 1F,H); however, the retrotympanic process of the squamosal bone appeared intact.

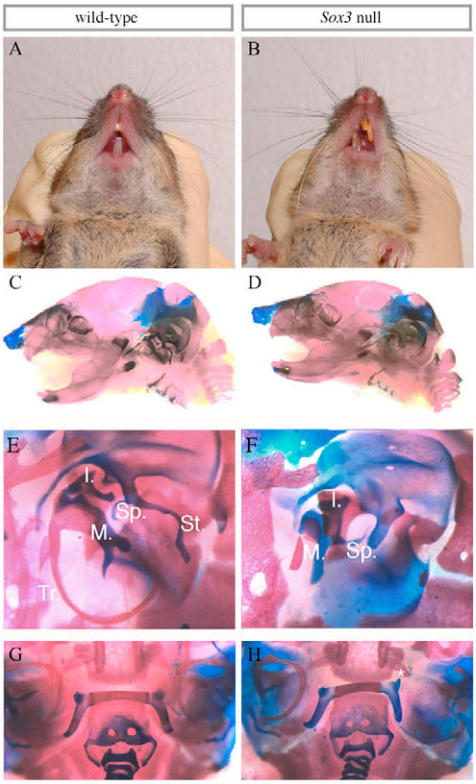

Fig. 1. Craniofacial defects in *Sox3* null mice. (**A**) Wild-type mouse. (**B**) *Sox3* null mouse with teeth overgrowth and vibrissae paralysis on the left side. (**C-H**) Skeletal preparation of wild-type (C) and *Sox3* null (D) newborns. Higher magnification of the middle ear in a control (E) and mutant (F), where the tympanic ring and distal part of the styloid bone are absent and the stapes and distal part of the malleus are malformed. Magnification of the hyoid bone in wild-type (G) and mutant (H) newborn with abnormal orientation of the lesser horn (asterisk) on the left side. (**I**) Statistical analysis of the craniofacial skeletal defects in *Sox3* null mice (n=14). I, incus; M, malleus; Sp, stapes; St, styloid process; Tr, tympanic ring.

I

		Right	Left
1st Arch derived elements	Tympanic ring	7% reduced	7% reduced on both sides (1/14) 7% reduced 7% absent
	Incus	-	-
	Malleus	7% reduced	35.7% distal part reduced 7% absent
	Stapes	35.7% reduced 7% absent	42.9% reduced 21.4% absent
2nd Arch derived elements	Styloid process	35.7% reduced or partially formed	85.7% reduced or partially formed
	Hyoid bone	-	42.8% lesser horn abnormally orientated

The external and the middle ear develop from PA1 and 2 (Mallo, 2001), with ncc in the latter giving rise to Reichert's cartilage, which forms the stapes, styloid process, lesser horn part of the hyoid bone and the processus brevis (O'Gorman, 2005). It has also been hypothesised that the facial mimetic musculature could be of PA2 ncc origin (O'Gorman, 2005), which could explain the impairment of vibrissae mobility seen in some mutants. As the elements most significantly affected in *Sox3* null animals were directly derived from PA2 ncc or consistent with a PA2 defect, we focused on PA2 development.

SOX3 is required for neural crest cell migration in PA2

We first looked at ncc migration with whole-mount immunofluorescence for CRABPI at 9.5 dpc (20/25 somites). At this stage ncc from r4 and r6/7 are migrating respectively into PA2 and 3 (Fig. 2C). By contrast, in mutant embryos, ncc migration into PA2 was initiated but then disrupted as cells entered the arch, the proximal domain of which was hypomorphic (Fig. 2D, arrow), whereas migration into PA3 appeared normal. The penetrance (around 60% of the embryos were affected, n=20) and severity of the

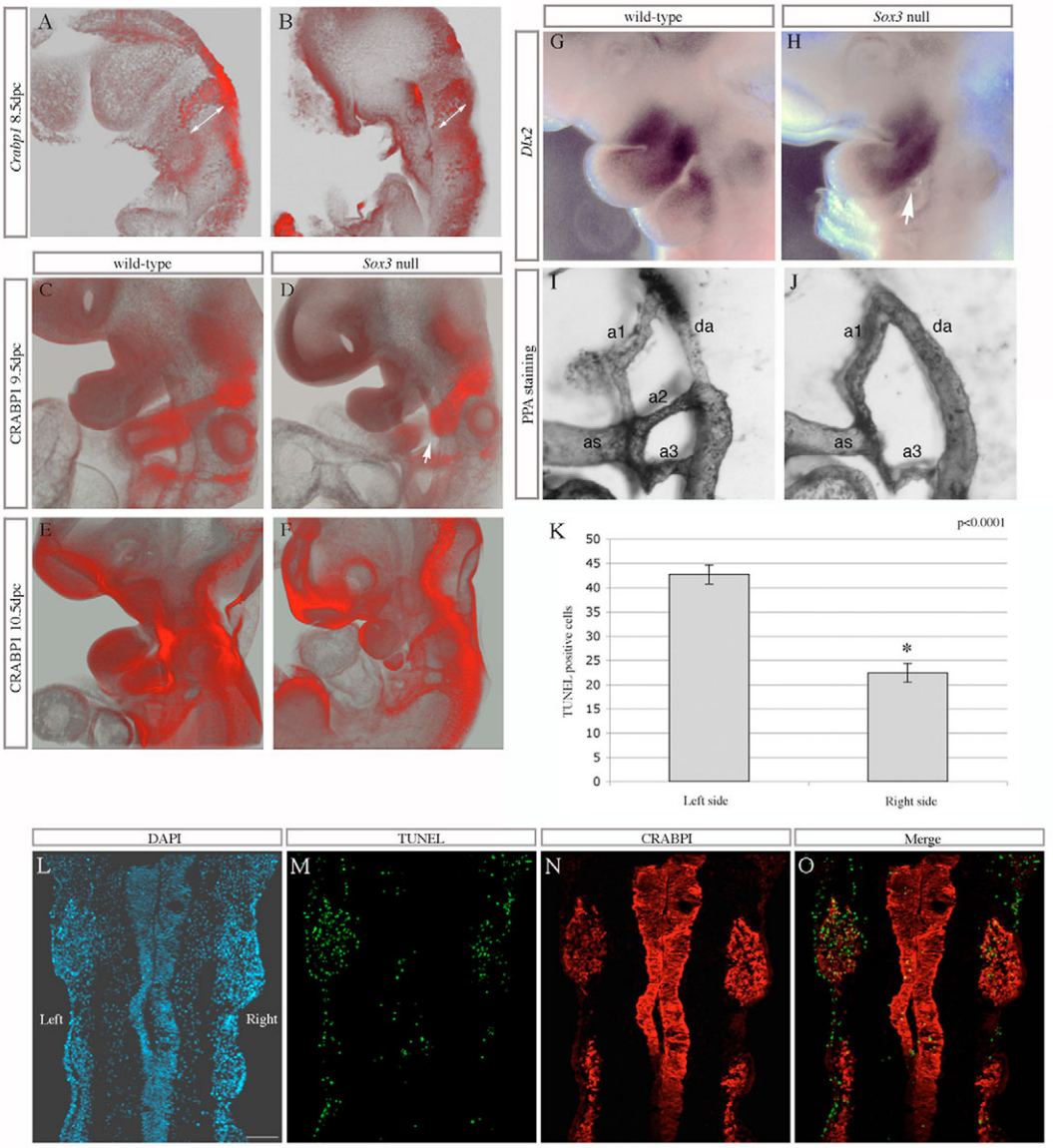

Fig. 2. Ncc migration defect in *Sox3* null mouse embryos. (**A-F**) CRABPI immunofluorescence and 3D reconstruction. (A,B) *Sox3* null embryo at 10 ss: only confocal sections through the region containing migrating ncc were used for 3D reconstruction (to avoid foregut diverticulum background). (A) Right side with PA2 migrating ncc. (B) Left side with ncc accumulating in front of PA2 (compare distance covered by ncc between both sides, arrows). (C) Wild-type and (D) *Sox3* null embryo at 9.5 dpc, with ncc accumulating in front of PA2 (arrow). Staining is present in the distal part of the arch. (E) Wild-type and (F) *Sox3* null embryo at 10.5 dpc with hypoplastic PA2. The bulge of ncc observed at 9.5 dpc is strongly reduced. (**G**,**H**) *Dlx2* in situ hybridisation on 10.5 dpc wild-type (G) and *Sox3* null embryos (H): reduction of Dlx2 staining in proximal PA2 (arrow). (**I**,**J**) PAAs staining by ink injection in wild-type (I) and *Sox3* null (J) 9.5 dpc embryos, where PAA2 is missing. (**K**) Apoptosis quantification. An average of 42.7±1.95 CRABP/TUNEL-positive cells were present on the left side of affected embryos, whereas we counted 22.45±2 on the right side (P<0.0001, n=7). (**L-O**) TUNEL assay and CRABPI immunofluorescence. Coronal section of 9.5 dpc *Sox3* null embryo affected on the left side only. DAPI (L). TUNEL assay (M). CRABPI (N). TUNEL/CRABPI merge picture (O). More apoptotic ncc are present on the left side of the embryo. Scale bar: 75 μm in L for L-O. a1-3, pharyngeal arch arteries 1-3; as, aortic sac; da, dorsal aorta.

defects were variable and occurred mainly on the left side, in agreement with the asymmetric nature of the skeletal defects. Some CRABPI staining was, however, present in the distal part of PA2 even in severely affected mutants, showing that some ncc still reach their destination (Fig. 2D). Two hypotheses could explain this observation. First, early migrating ncc are known to populate the distal part of the arches (Serbedzija et al., 1992). Therefore, the defect could arise subsequently to this initial migration phase, just after the 10-somite stage (ss). Alternatively, ncc migration could be disrupted from its earliest phases, but only partially. We therefore performed CRABPI immunofluorescence during the early phase of ncc migration, between 10 and 12 ss. On the right side of a mutant embryo, the first ncc had reached PA2, whereas on the left side many of the crest cells were already disrupted in their migration (Fig. 2A,B). Therefore, the ncc defect is present from the earliest stages and the residual staining seen in PA2 shows that entry into the arch is only partially disrupted. This experiment also showed that ncc migration in the first PA is unaffected.

At 10.5 dpc CRABPI immunostaining revealed ncc migrating into PA3 and 4 in both wild-type and mutant embryos, on both sides (Fig. 2E,F). The hypoplastic appearance of PA2 was very obvious in the mutants at this stage. However, compared with 24 hours earlier (Fig. 2D), the crest cells accumulating in front of PA2 in the mutant embryos had almost disappeared. As the proximal region of the arch had an abnormal morphology at 9.5 dpc, we also examined the expression of *Dlx2*, present at 10.5 dpc in the mesenchyme all along the proximodistal axis of PA1 and 2 (Bulfone et al., 1993). In mutant embryos, the proximal region of PA2 did not show any staining, whereas the reduced distal part of the arch still expressed *Dlx2* (Fig. 2G,H). This is consistent with the abnormal morphology of this region at 9.5 dpc and shows that post-migratory ncc and mesenchyme are largely absent from the proximal part of PA2. We also examined pharyngeal arch arteries (PAA) at 9.5 dpc as they originate from ncc and mesenchyme. We found that PAA2 was missing in phenotypically affected mutants (Fig. 2I,J). Analysis at 10.5 dpc did not reveal defects in more posterior PAA (data not shown, *n*=15).

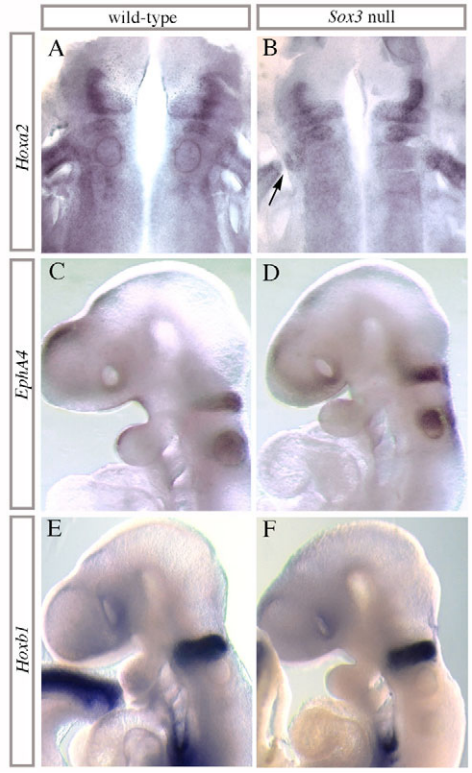

Fig. 3. Marker analysis in the mouse hindbrain at 9.5 dpc. (**A**,**B**) *Hoxa2* in situ hybridisation on flat mounted hindbrain in wild-type (A) and mutant (B) embryos. (B) Arrow points to the abnormal proximal pa2 on the left side. (**C**,**D**) *EphA4 in situ* hybridisation in wild-type (C) and mutant (D) embryos. (**E**,**F**) *Hoxb1* in situ hybridisation in wild-type (E) and mutant (F) embryos. No significant difference was observed in the mutants for these three markers.

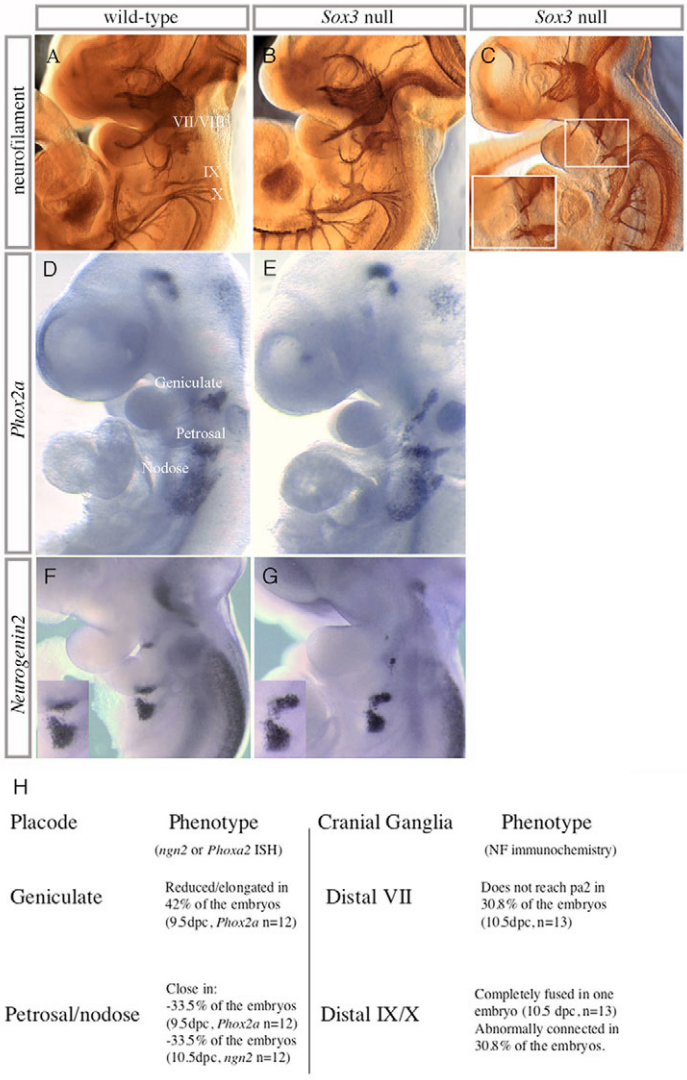

Fig. 4. Cranial nerves and epibranchial placode formation in mice. (**A-C**) Anti-neurofilament immunochemistry at 10.5 dpc. Wild-type embryo (A). (B) *Sox3* null embryo with a fusion of the IX and X cranial nerves. (C) *Sox3* null embryo, in which nerves from the distal VII and IX ganglia do not reach PA2 and PA3, respectively (inset corresponding to the boxed region). (**D**,**E**) *Phox2a* in situ hybridisation at 9.5 dpc, showing the epibranchial placodes. (D) Wild type. (E) *Sox3* null embryo with a reduced geniculate placode and a fusion of the petrosal and nodose placodes. (**F**,**G**) *Ngn2* in situ hybridisation at 10.5 dpc. (F) Wild-type embryo (magnification of petrosal/nodose placodes, inset). (G) *Sox3* null embryo, in which petrosal and nodose placodes are connected (magnification, inset). (**H**) Statistical analysis of the placodal and cranial nerves defects in *Sox3* null embryos.

Neural crest cells accumulating at 9.5 dpc die by apoptosis in *Sox3* mutants

A plausible explanation for the absence of *Dlx2* staining in proximal PA2 and of PAA2 is that the ncc die. We therefore performed TUNEL assays on 9.5 dpc sections, coupled with CRABPI immunofluorescence, taking advantage of the asymmetric nature of the defect by selecting mutant embryos affected exclusively on the left. We then compared the cell death pattern on both sides of the same embryo using the unaffected right side as control (Fig. 2K-O). The average number of TUNEL-positive cells on the left was almost double that of the right (Fig. 2K). Therefore, in *Sox3* null embryos, ncc disrupted in their migration toward PA2 die by apoptosis at 9.5 dpc.

Sox3 deletion in the CNS is unlikely to be the origin of the craniofacial defects

Although absent in migrating ncc, *Sox3* is widely expressed in the CNS at 9.5 dpc and deletion of the gene could affect hindbrain development and/or have consequences on ncc precursors. We first looked at the expression of *Hoxa2*, present in PA2 ncc and in the hindbrain from r2 (Fig. 3A,B), at *EphA4*, expressed in r3 and r5 (Fig. 3C,D), and *Hoxb1*, an r4 marker (Fig. 3E,F). No significant differences were seen between wild-type and mutant embryos for these three markers, suggesting that ncc regional identity and hindbrain patterning are not significantly altered in *Sox3* null embryos.

To directly examine any role for SOX3 in ncc precursors, *Wnt1-Cre* was used to delete *Sox3* specifically in these cells (Danielian et al., 1998). We did not observe any PA2 defects, either in $Sox3^{Yflox.gfp}$; *Wnt1-Cre* embryos at 9.5 dpc (n=6) or adults (n=14) (data not shown). It is therefore very unlikely that the lack of SOX3 in the CNS, including ncc precursors, is responsible for the phenotype.

SOX3 is also expressed in the pharyngeal region, the formation of which relies in particular on the endoderm. As the latter induces the epibranchial placodes from which the distal cranial ganglia derive, we examined their development in the *Sox3* null mutants, in order to highlight any potential pharyngeal defects.

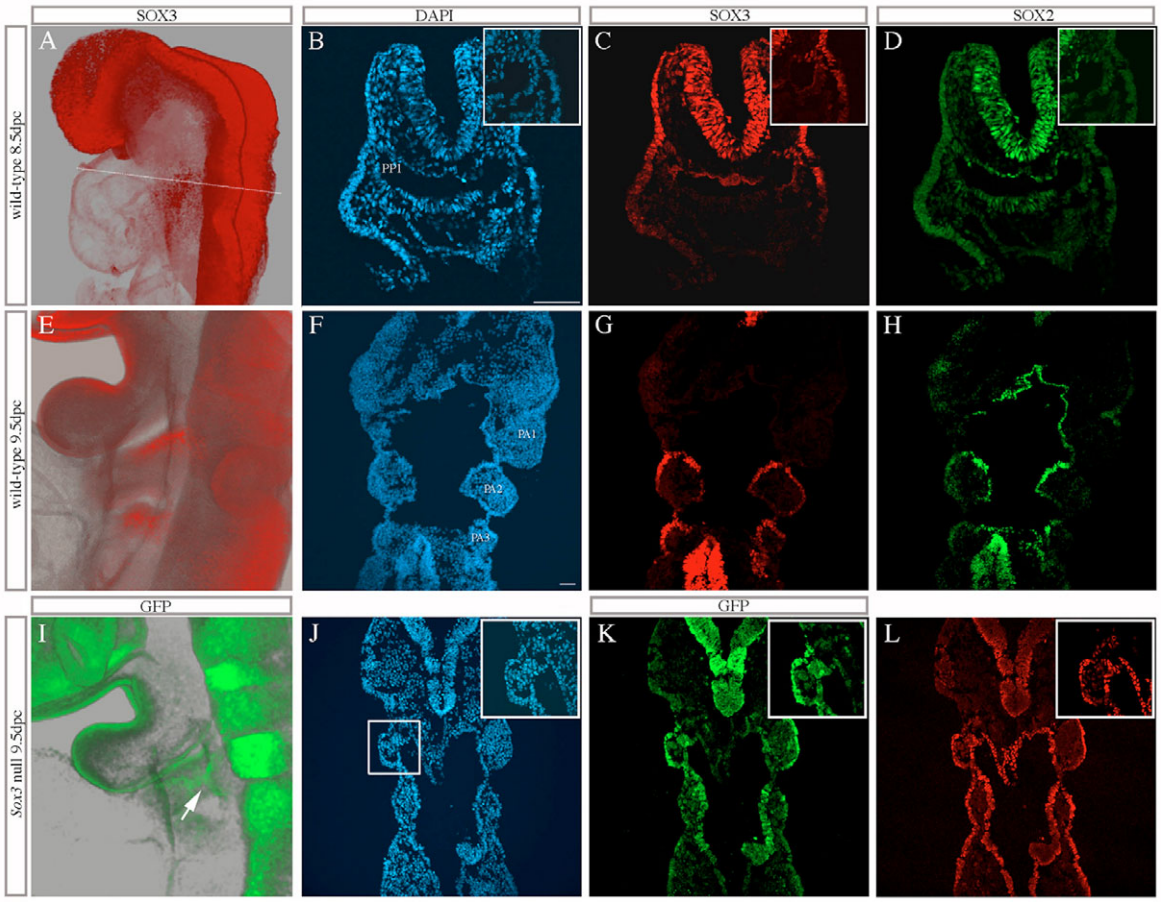

Fig. 5. SOX3 and SOX2 expression in the pharyngeal region in wild-type and mutant mouse embryos. (**A,E,I**) Whole-mount immunofluorescence and 3D reconstruction of embryo sagittal halves. (**B-D,F-H,J-L**) Immunofluorescence on sections. (A,E) Anti-SOX3 immunofluorescence. (A) Expression at 8 ss in the neural plate and pharyngeal region. (B-D) Transverse section at 8-10 ss at PP1 level (section plan shown in A). (B) DAPI. (C) SOX3 is detected in the proximal pharyngeal ectoderm and underlying lateral endoderm (note non-specific staining in foregut diverticulum); inset magnified PP1 region boxed. (D) SOX2 is present more widely than SOX3 in the pharyngeal endoderm. (E) At 9.5 dpc SOX3 expression is restricted to the posterior pouch margins. (F-H) Coronal section in the proximal pharyngeal region at 9.5 dpc. (F) DAPI. (G) SOX3 is detected in both epithelia in the posterior pouch margin. This regionalisation is acquired as the arches develop: in the more caudal PA3, SOX3 expression is not as restricted as in PA2. (H) SOX2 is present in the pharyngeal endoderm and weakly in the ectoderm. (I) Anti-GFP immunofluorescence on a *Sox3* null embryo at 9.5 dpc. GFP (from the *Sox3* locus) is present across the reduced proximal region of PA2 (arrow). (J-L) Coronal section in the proximal pharyngeal region at 9.5 dpc in a *Sox3* null embryo. (J) DAPI staining (inset: magnified abnormal PA2, boxed). (K) GFP is present all around the hypomorphic proximal region of PA2. (L) SOX2 expression also highlights the abnormal morphology of PA2 (expression is stronger in the ectoderm than in H as the section is more distal). Scale bars: 50 μm in B, for B-D; in F, for F-H and J-L.

SOX3 is necessary for cranial nerve and epibranchial placode formation

We first examined the cranial nerves in mutants by anti-neurofilament immunochemistry at 10.5 dpc (Fig. 4A-C,H). In a third of the embryos (n=13), where PA2 defects were clearly apparent, nerves from the distal VII ganglia did not reach the arch. This could be explained by the nearly complete physical separation of the arch (Fig. 4C inset). Some of these embryos displayed similar defects at the level of IX ganglia, with nerves failing to reach PA3 (Fig. 4C). This arch could be affected in a similar way to PA2, although with less penetrance, explaining the nerve defect. We also observed fusion of nerves IX and X, complete in one case (Fig. 4B) but less severe in a further 30%.

We then looked at the epibranchial placodes by *Phoxa2* in situ hybridisation at 9.5 dpc (Fig. 4D,E,H). The geniculate contributes to the distal VII ganglia, but in 42% (n=12) of mutant embryos we observed a reduction and elongation of this placode (Fig. 4E), expected as it forms in the region most affected by *Sox3* deletion (Fig. 2). Moreover, while in wild-type embryos the nodose and petrosal placodes were separated, they appeared abnormally close in 42% of *Sox3* null embryos. As confirmation of this result, *ngn2* in situ hybridisation at 10.5 dpc revealed contact between them in some mutants (Fig. 4F,G, insets). This defect is likely to reflect a reduction of the region encompassing proximal PA3 and PP3 as the placodes form on each side of this domain. These observations were consistent with fusion of the IX and X distal nerves, deriving respectively from petrosal and nodose placodes.

In conclusion, as the VII ganglia innervate the face, defects affecting the growth of these nerves in *Sox3* mutants could explain the vibrissae paralysis in a subset of animals. Furthermore, the defects in the epibranchial placodes suggest that the pharyngeal region is affected. We therefore examined SOX3 expression in the PA.

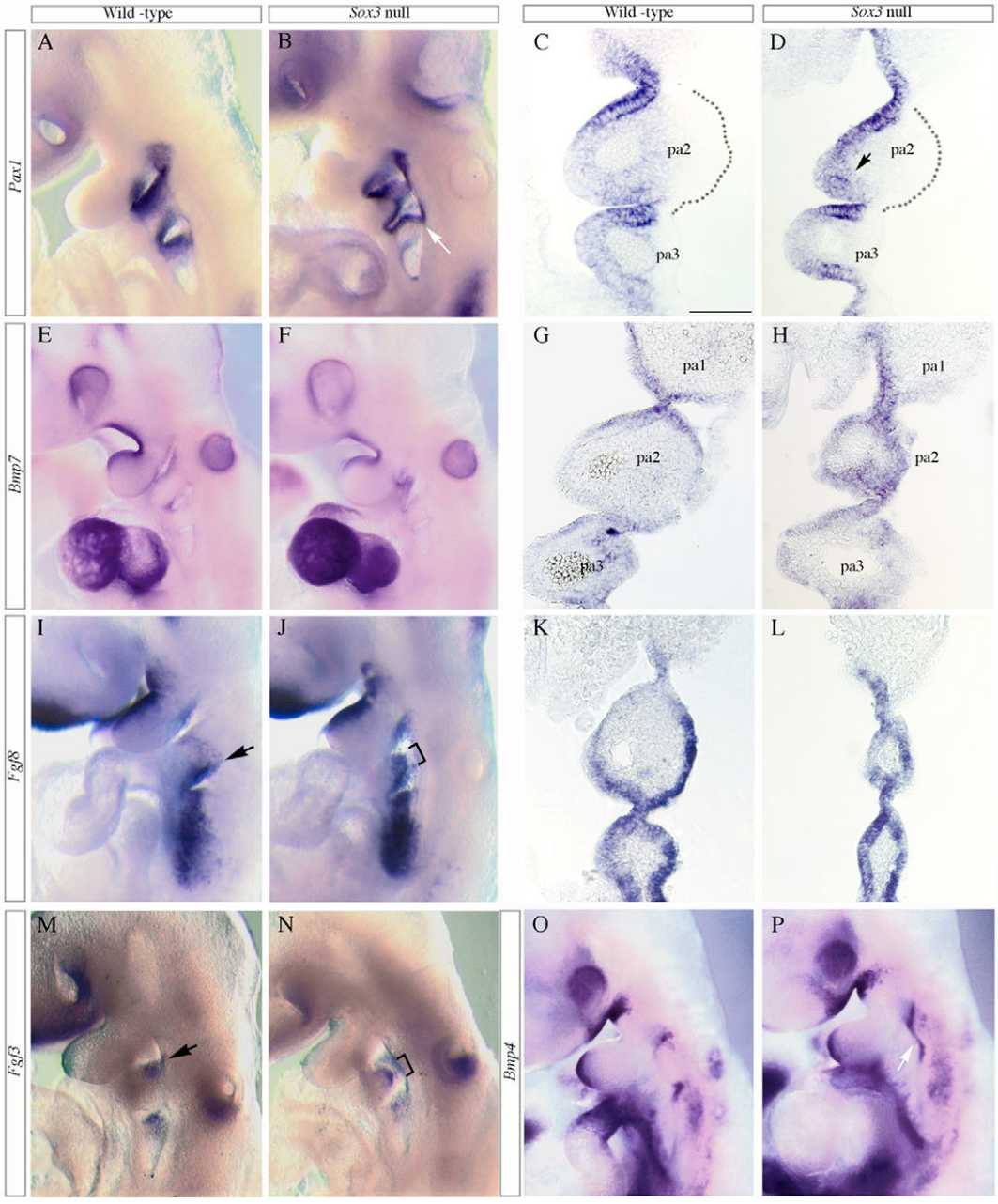

Fig. 6. Marker analysis in mouse pharyngeal pouches at 9.5 dpc. (**A**,**B**) *Pax1* in situ hybridisation in wild type (A) and *Sox3* null (B) embryos. Note the abnormal appearance of proximal PA3 (arrow). (**C**,**D**) Coronal sections through the proximal pharyngeal region of wild-type (C) and *Sox3* null (D) embryos hybridised with *Pax1*. The domain of expression is expanded throughout PA2 endoderm (arrow). (**E**,**F**) *Bmp7* in situ hybridisation in wild-type (E) and *Sox3* null (F) embryos. (**G**,**H**) Coronal sections of wild-type (G) and *Sox3* null (H) embryos hybridised with *Bmp7*. (**I**,**J**) *Fgf8* in situ hybridisation in wild type (I) in the anterior pouch margin (arrow) and *Sox3* null embryo (J), where it is present across the reduced PA2 (bracket). (**K**,**L**) Coronal sections of wild-type (K) and *Sox3* null (L) embryos hybridised with *Fgf8*. (**M**,**N**) *Fgf3* in situ hybridisation in wild type (M) in the posterior pouch margin (arrow) and *Sox3* null embryo (N), where it is present across the reduced PA2 (bracket). (**O**,**P**) *Bmp4* in situ hybridisation in wild-type (O) and *Sox3* null (P) embryos with uninterrupted expression between first and second pharyngeal clefts, arrow. All these markers of the pouch endoderm and/or ectoderm show an expansion of their expression across proximal PA2 in the mutant embryos. Scale bar: 100 μm in C for all sections.

SOX3 and SOX2 start to be expressed early in the pharyngeal epithelia

Sox2 and *Sox3* are both expressed in the pharyngeal region (Wood and Episkopou, 1999). At 8/9 ss the rostral limit of SOX3 expression was the PA2 domain, both in the ectoderm covering the future arch and in the endoderm, albeit laterally restricted in the latter (Fig. 5A-C). At this stage, SOX2 (Fig. 5D) was expressed more widely than SOX3, being present in a continuous domain of head and pharyngeal ectoderm and generally in the endoderm. When PP1 was fully formed (20/25 somites), SOX3

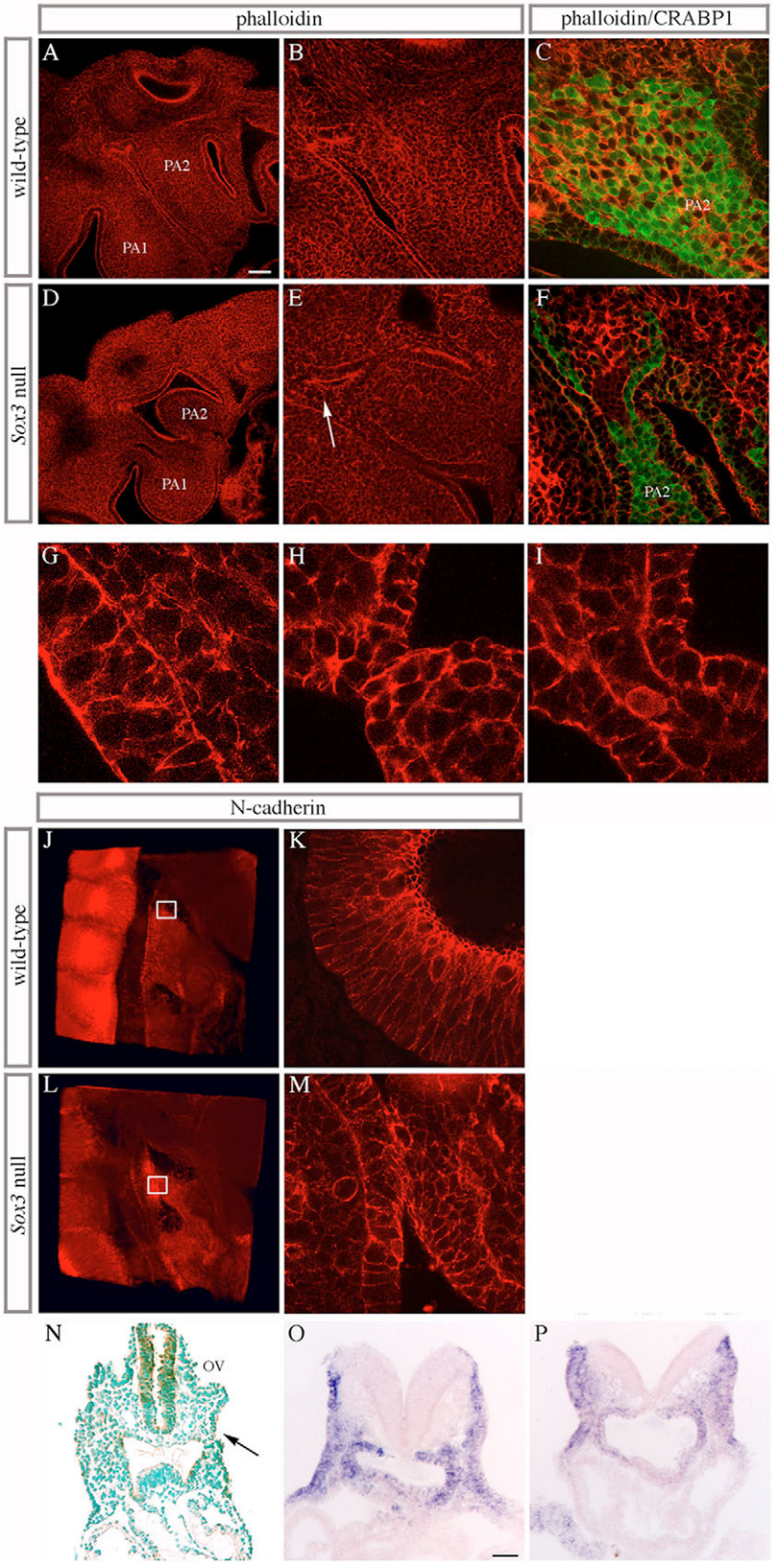

Fig. 7. Morphology of proximal PA2 in *Sox3* null mouse embryos. (**A,B,D,E,G-I**) Confocal sections of phalloidin-stained 9.5 dpc wild-type (A) and *Sox3* null (D) embryos. PP1 and PP2 appear connected in the mutant. (B,E) Higher magnification and deeper sections of a wild-type (B) and *Sox3* null (E) embryos with a 'stem' connecting distal PA2 (arrow). (C,F) Confocal sections of phalloidin and anti-CRABPI double-stained 9.5 dpc wild-type embryo (C) and *Sox3* null mutant (F), where ncc migrate through the 'stem'. (G-I) High magnification of PP1 posterior margin in wild type (G) and of the 'stem' in mutant embryos (H,I). Superficial section (H), where margin-like cells form a 'stem' but show a disruption of apical actin accumulation. Deeper section (I), where two margins flank what is left of PA2. Actin polarisation is also disrupted. (J-M) Anti-N-cadherin immunofluorescence on 9.5 dpc embryos. (J) 3D reconstruction of a wild-type embryo sagittal half, inside view. Expression is seen in the neural tube and pharyngeal endoderm. (K) High magnification of a confocal section (region boxed in H) with apical accumulation of N-cadherin in the pouch margin. (L) 3D reconstruction of a mutant embryo sagittal half, inside view. (M) High magnification of confocal section (region boxed in J) with a disruption of apical N-cadherin accumulation. (N) Anti-GFP immunohistochemistry of a 17 ss *Sox3* null embryo (transverse section, PA2 level). The close apposition between ectoderm and endoderm on one side (arrow) interrupts PA2. (O,P) *Spry-1* in situ hybridisation on 8/9 ss wild-type (O) and 7/8 ss *Sox2*$^{+/-}$; *Sox3*$^{Y/-}$ (P) embryos sectioned at pharyngeal level, posterior to PA1; the gene is expressed in pharyngeal epithelia and mesenchyme. No significant difference is observed between wild type and double mutant. Scale bar: 100 μm in A for A,D; 50 μm for B,E and O,P; 25 μm for C,F; 10 μm for G,H,I,K,M. ov, otic vesicle.

Table 1. Ncc migration defects in *Sox2; Sox3* double mutants

Genotype	Abnormal ncc migration			
	Right	Left	Both	% total defect
Sox2$^{+/-}$	–	–	–	0.0 (*n*=11)
Sox3$^{+/-}$	–	1	–	11.1 (*n*=9)
Sox3$^{-/\gamma}$ *or Sox3*$^{-/-}$	–	7	6	76.4 (*n*=17)
Sox2$^{+/-}$; *Sox3*$^{+/-}$	–	2	1	50.0 (*n*=6)
Sox2$^{+/-}$; *Sox3*$^{-/\gamma}$	–	1	5	100.0 (*n*=6)

Migration defects were analysed at 9.5 dpc by CRABPI in situ hybridisation. Embryos were littermates obtained from *Sox3*$^{+/-}$ females mated with *Sox2*$^{+/-}$ males. Removing one copy of *Sox2* on the *Sox3* mutant background increases both penetrance and severity of the ncc defects. ncc, neural crest cell.

expression was further restricted to its posterior margin and the flanking ectoderm and endoderm covering the anterior half of PA2 (Fig. 5E-G). SOX2 was expressed more widely throughout the pharyngeal endoderm (Fig. 5H), whereas in the ectoderm its expression was stronger distally (compare Fig. 5H, proximal, with Fig. 5L, more distal). Levels of expression between right and left sides were compared for both genes by quantitative RT-PCR on right and left pharyngeal explants at 9.5 dpc. No significant difference was observed (*n*=4 embryos, no difference for *Sox3*, *P*=1, no difference for *Sox2*, *P*=0.3).

SOX3 is required for maintenance/identity of proximal PA2

Pouch morphology was then examined in 9.5 dpc *Sox3* null embryos using anti-GFP immunofluorescence. In PA2, the hypomorphic proximal region showed continuous GFP staining (Fig. 5I,K). An abnormal mass of GFP-positive cells was visible in rostral PA2 (Fig. 5K, inset). SOX2 staining highlighted PA2 defects and also suggested that the SOX3-negative, GFP-positive cells had retained their ectodermal and endodermal epithelial identities as SOX2 and GFP colocalised. These results also suggested that the proximal part of PA2 had been dramatically reduced at the benefit of an enlarged pouch margin. This is the epithelium delineating the pouches that forms as a result of a localised apposition of pharyngeal ectoderm and endoderm. The continuous or ectopic formation of such a structure in the proximal region of PA2 would result in narrowing and a physical disruption of ncc migration. In order to test this hypothesis, we looked first at the expression of markers of this compartment at 9.5 dpc.

Pax1 and *Bmp7* are normally expressed in the PP margins, in the endoderm and both epithelia, respectively (Fig. 6A,C,G,E). In mutants, the narrowed proximal second arch showed continuous staining of both markers, between PP1 and PP2 (Fig. 6B,D,F,H). The defects were even more apparent in coronal sections (Fig. 6D, arrow, Fig. 6H).

Fgf3, like SOX3, was expressed in both the endoderm and ectoderm in posterior pouch margins (Fig. 6M), while *Fgf8* was present in the anterior pouch margin, again in both layers (Fig. 6I,K). In *Sox3* null embryos, however, both genes were expressed across the proximal PA2, suggesting that the polarity of this domain is also affected (Fig. 6J,L,N).

Bmp4 is present in the ectoderm of the cleft region of PA1 and 2 (Fig. 6O). In *Sox3* null embryos, an uninterrupted *Bmp4*-positive region expanded across the two first PP (Fig. 6P). This extended the results observed with the endodermal markers to PA2 proximal ectoderm.

These results support the notion that the proximal region of PA2 is replaced by, or re-specified as, an aberrant pouch margin. Moreover, the anteroposterior polarity of this domain has been lost. This marker analysis also revealed morphological defects in the proximal region of PA3 (arrows, Fig. 6B), with less penetrance than those affecting PA2. PA1 was not affected, however, which is consistent with the rostral limit of SOX3 expression in presumptive PA2 (Fig. 5A,D). Finally, we examined PP3 endoderm by performing CasR in situ hybridisation and did not observe any significant anomaly even in severely PA2-affected mutants (data not shown, *n*=10), suggesting that the defects were restricted to the region encompassing PP1 and 2. Moreover, histological examination of the parathyroid/thymus primordia at 11.5 dpc did not reveal any significant defect in the mutants (data not shown).

Proximal PA2 morphology is abnormal without SOX3

Pharyngeal pouch elongation in chick relies on a network of actin fibres localised apically within the pouch endoderm (Quinlan et al., 2004). We therefore examined this network to analyse in more detail endodermal margin cells as the pouches formed. In wild-type embryos, apical accumulation of actin was easily visible in pouch margins using phalloidin staining, as initially reported in chick (Fig. 7A-C,G). In severely affected *Sox3* null embryos, this staining highlighted the PA2 phenotype: the actin network was organised as if an uninterrupted pouch margin was present on the proximal side, connecting PP1 and 2. However, sections taken deeper in the arch revealed the presence of a ‘stem’ connecting the distal arch (Fig. 7E, arrow, F,H,I). Double CRABPI/phalloidin staining showed that this stem is the route by which a reduced stream of ncc enter the arch (Fig. 6F). At high magnification deeper within the stem, two margins flank what could be a residual proximal PA2, but actin polarisation is clearly disrupted (Fig. 7H,I).

We then examined the distribution of N-cadherin associated with these actin cables (Quinlan et al., 2004) (Fig. 7J,L). At high magnification, there is a clear apical accumulation in the pouch margin of wild-type embryos (Fig. 7K), but this was not seen in *Sox3* null embryos, where instead it was homogeneously distributed within the abnormal margin cells (Fig. 7M).

In conclusion, in *Sox3* null embryos, endodermal and ectodermal cells seem to be organised in a margin, but they do not retain their morphological characteristics, namely apical actin accumulation associated with N-cadherin; they form an enlarged but abnormal epithelium at the detriment of the proximal region of the arch, which is essentially reduced to a ‘stem’, allowing migration of only a few ncc.

In order to understand the origin of these defects, we examined mutant embryos at 8/8.5 dpc, as SOX3 is expressed in the presumptive PA2 domain when pharyngeal segmentation takes place.

SOX3 is required early during pharyngeal segmentation

We first performed anti-GFP immunohistochemistry to examine the pharyngeal epithelia in mutants. The morphological defect was initially seen at the time the first pharyngeal membrane had formed

Table 2. External ear phenotype in *Sox3; Fgfr1* double mutants

Genotype	Affected ear			
	Right	Left	Both	% total defect
$Fgfr1^{n7/+}$	–	–	–	0.0 (*n*=24)
$Sox3^{+/-}$	–	–	–	0.0 (*n*=24)
$Sox3^{-/y}$ or $Sox3^{-/-}$	1	2	–	18.8 (*n*=16)
$Sox3^{+/-}$; $Fgfr1^{n7/+}$	2	4	2	20.5 (*n*=39)
$Sox3^{-/y}$ or $Sox^{-/-}$; $Fgfr1^{n7/+}$	1	1	7	90 (*n*=10)

Defects were monitored after weaning on littermates obtained either from $Fgfr1^{n7/+}$ mated with $Sox3^{-/y}$ or $Sox3^{+/-}$; $Fgfr1^{n7/+}$ mated with $Sox3^{-/y}$. Introduction of the hypomorphic *Fgfr1* allele leads to the appearance of defects in $Sox3^{+/-}$ females and increases their penetrance in $Sox3^{-/y}$ and $Sox3^{-/-}$ animals.

(9/11 somites, data not shown) and appeared as a prolonged region of contact in the rostrocaudal axis between the ectoderm and the endoderm, interrupting PA2. On the embryo shown in Fig. 7N, clearly separated ectoderm and endoderm, corresponding to the proximal region of PA2, through which ncc are known to migrate, were seen in only two consecutive sections on one side but eight on the other, and the proximal region of the arch was reduced to closely apposed/intermingled layers of ectodermal and endodermal GFP-positive cells. This prolonged contact zone between these two layers is likely to prefigure the formation of the enlarged pouch margin and explains the reduction of the PA2 domain. To discriminate between an endodermal and/or ectodermal origin of the *Sox3* null phenotype, further conditional deletions will be necessary. We tested the Tbx1Cre driver (Brown et al., 2004), but this is expressed in the head mesenchyme at 8.5 dpc, not in the epithelia, which explains why we did not observe any PA2 defect. The Foxg1Cre driver (Hebert and McConnell, 2000), expressed in the pharyngeal endoderm, was also tested, but gave rise to ectopic activity on our genetic background.

As SOX3 is involved in proliferation of neuroepithelial progenitors in the ventral diencephalon (Rizzoti et al., 2004), we looked at this and cell death in the endoderm of PA2 at 8.5 and 9.5 dpc. No differences were found between wild-type and mutant embryos (data not shown), which is consistent with SOX3 being required for cell fate or morphology.

Sox3 genetically interacts with *Sox2* and *Fgfr1* during PA2 development

Because SOX2 is expressed in the pharyngeal region, in a partially overlapping pattern with SOX3 (Fig. 5), we looked for a genetic interaction. Animals heterozygous for a *Sox2* null mutation do not present any craniofacial defects [homozygotes die around implantation (Avilion et al., 2003)]. *Sox3* heterozygotes only very rarely present defects, while in hemizygotes these vary in severity. We therefore examined the effects of removing one copy of *Sox2* in *Sox3* heterozygous and hemizygous mutants. As $Sox2^{+/-}$; $Sox3^{+/-}$ animals have a reduced viability and $Sox2^{+/-}$; $Sox3^{Y/-}$ die in utero (K.R., unpublished) we examined ncc migration in mutant embryos by *CRABPI* in situ hybridisation at 9.5 dpc. Removing one copy of *Sox2* increased both the penetrance and severity of the defects, with the majority of $Sox2^{+/-}$; $Sox3^{Y/-}$ embryos being affected symmetrically (Table 1). This genetic interaction is likely to represent functional redundancy between the closely related proteins encoded by the two genes.

Mutations in *Fgfr1* induce a phenotype similar to that of *Sox3* mutants (Trokovic et al., 2003; Trokovic et al., 2005). We therefore explored genetic interactions with this gene in two ways. First, as with $Sox3^{+/-}$ mutants, heterozygotes for a hypomorphic mutation in *Fgfr1* ($Fgfr1^{n7/+}$) did not present craniofacial defects. We therefore looked at double heterozygotes ($Sox3^{+/-}$; $Fgfr1^{n7/+}$). Second, we asked if introduction of one hypomorphic *Fgfr1* allele on the *Sox3* null background would increase the penetrance of the defects. We conducted these tests postnatally, scoring external ear defects (Table 2), and in embryos, analysing ncc migration (Fig. 8). The penetrance of the defects was clearly increased in double mutant animals (Table 2) and embryos (Fig. 8). The PA2 phenotype was also more severe in *Sox3* null; $Fgfr1^{n7/+}$ embryos than in *Sox3* null embryos (Fig. 8B-E). Therefore, *Sox3* and *Fgfr1* interact during PA2 formation.

To characterise molecularly the interaction between *Sox3* and *Fgfr1*, we first checked the expression of *Fgfr1* in *Sox3* null embryos and of *Sox3* in $Fgfr1^{n7/n7}$ embryos. Both appeared normal (data not shown). To assess FGF signalling in our mutants, we looked for the downstream target *Sprouty-1* (*Spry-1*), the expression of which is downregulated in the ectoderm of $Fgfr1^{n7/n7}$ embryos before the phenotype is morphologically apparent at 8.5 dpc (Trokovic et al., 2005). Because of the variable penetrance of the PA2 phenotype in our mutants, we decided to check *Spry-1* expression in $Sox2^{+/-}$; $Sox3^{Y/-}$ embryos, where defects are more severe and the penetrance is close to 100% (Table 1). In situ hybridisation for *Spry-1* on 7 to 11 ss double mutant embryos did not reveal any significant downregulation of the FGF signalling target specifically in the ectoderm (Fig. 7O,P). We also examined *Sox3* null embryos for expression of the phosphorylated form of ERK as a readout of FGF activity, but we were unable to detect any significant alteration between mutants and controls at 8.5 and 9.5 dpc (data not shown). Finally, we checked the expression of *Fgf3* and *Fgf15*, which are both downregulated in *Fgfr1* hypomorphs, but again failed to see any significant reduction.

In conclusion, SOX3 is required for the development of the second arch, where it genetically interacts both with the closely related *Sox2*, probably by redundancy, and also *Fgfr1*, linking the activity of SOXB1 proteins in this region with FGF signalling.

DISCUSSION

Deletion of *Sox3* in mice results in a range of defects, including those within the CNS that lead to hypopituitarism, in spermatogenesis and in craniofacial development (Raverot et al., 2005; Rizzoti et al., 2004; Weiss et al., 2003). Here we present evidence suggesting that the latter arise from a requirement for SOX3 within the pharyngeal epithelia, where it is present from early stages. In support of this hypothesis, deletion of the gene in ncc precursors, where it is normally expressed, does not explain the occurrence of the defects. By contrast, in the complete absence of SOX3, pharyngeal segmentation is disrupted and, probably as a consequence, epibranchial placode development is compromised. The proximal domain of PA2 is predominantly affected, leading to a constriction that disrupts migration of r4 ncc into the arch. These ncc then die by apoptosis and elements almost exclusively derived from PA2 are incomplete or missing, resulting in craniofacial defects. We also show that *Sox3* interacts genetically with *Sox2* and *Fgfr1* for PA2 formation, providing new insight into the cascade of events underlying pharyngeal segmentation, and hence craniofacial development.

A

Genotype \ Abnormal ncc migration	Right	Left	Both	% Total defects
$FgfR1^{n7/+}$	-	-	-	0%, n=10
$Sox3^{+/-}$	1	-	-	11%, n=10
$Sox3^{Y/-}$	-	2	1	37.5%, n=8
$Sox3^{+/-};FgfR1^{n7/+}$	2	2	-	57%, n=7
$Sox3^{Y/-};FgfR1^{n7/+}$	-	3	6	90%, n=10

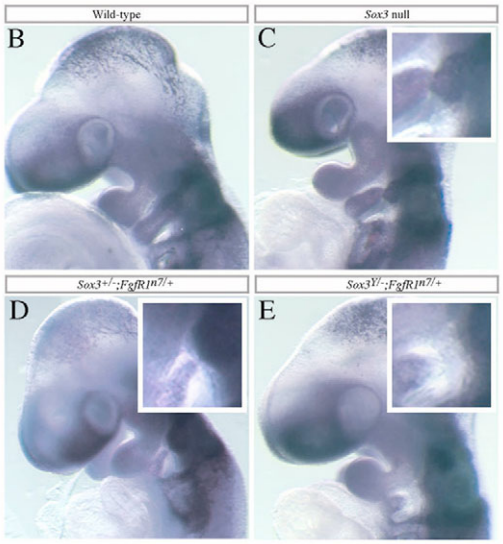

Fig. 8. Ncc migration defects in *Sox3*; *Fgfr1* double mutants. (**A**) Migration defects were analysed at 9.5 dpc by *Crabpl* in situ hybridisation. Mouse embryos were littermates obtained from $Sox3^{+/-}$ females mated with $Fgfr1^{n7/+}$ males. Introduction of the hypomorphic *Fgfr1* allele increases the penetrance of the ncc defects on the *Sox3* mutant background. (Note: the penetrance of the *Sox3* null phenotype is reduced in this cross, perhaps due to the introduction of the different background on which the *Fgfr1* mutation is maintained, but the sample size is also small.) (**B-E**) *Crabpl* in situ hybridisation at 9.5 dpc on (B) wild-type, (C) *Sox3* null, (D) $Sox3^{+/-}$; $Fgfr1^{n7/+}$ and (E) *Sox3* null; $Fgfr1^{n7/+}$ embryos showing increasing severity of PA2 defects in double mutants. Insets: PA2 domain magnification.

SOX3 is required for pharyngeal segmentation

SOX3 is expressed in the pharyngeal region, extending caudally from the PA2 domain, at least from 8 ss, both in the endoderm and ectoderm. At 20/25 ss, it becomes restricted to the newly formed first posterior pouch margin and the flanking ectoderm and endoderm. In *Sox3* null mutants, as PA2 forms between 8 and 12 ss, we observed a prolonged region of apposition between the ectoderm and the endoderm that reduces the proximal region of the arch. Therefore, in the absence of SOX3, the identity/maintenance of the PA2 domain is compromised, such that the flanking pouches invade it as they form, consequently reducing the proximal domain to an aberrant pouch margin (Fig. 9). This suggests that the endoderm/ectoderm interaction underlying pouch formation in a wild-type presumptive arch domain must be spatially restricted so that each arch will emerge and be able to host migrating ncc. In our mutants, however, the expanded/ectopic margin is not an entirely normal epithelium, as the polarisation of actin and distribution of associated N-cadherin and β-catenin (data not shown) is disrupted. It also lacks a posterior or anterior pouch margin identity, showing that its anteroposterior patterning is affected. However, even in the most severe cases, proximal PA2 persists as a ‘stem’, allowing a few ncc to reach their destination.

We also observed PA3 defects, albeit with less penetrance and severity. We did not, however, see defects in the early parathyroid/thymus primordia, even though human patients with a translocation breakpoint upstream of SOX3 are affected by hypoparathyroidism (Bowl et al., 2005). This may reflect a role for SOX3 during subsequent development of this gland, in which its expression is maintained.

Variability and asymmetry of the phenotype

A general aspect of the *Sox3* mutant phenotype is its variability, both in penetrance and severity. This may be explained in part by functional redundancy with *Sox2*, as suggested by the interaction between the two genes (see also Wegner and Stolt, 2005). Double mutants for *Sox2* and *Sox3* might be expected to show even more severe defects, but this requires a conditional deletion of *Sox2*.

The genetic interaction of *Sox3* with *Sox2* and *Fgfr1* led not only to increased penetrance and severity, but also to more symmetrical defects in PA2. One obvious explanation for why the left side might be more ‘sensitive’ to the loss of SOX3 is that the protein is not expressed at the same level on both sides. We checked SOX3 expression levels by quantitative RT-PCR, but failed to observe any difference. The explanation is therefore more complex and tests of genetic interaction with known players in the establishment of left-right asymmetry will be required.

More generally this aspect of the phenotype emphasises that symmetric development of paired structures, such as the ears, is a regulated event. Such a feature has been observed in human patients affected by Holt-Oram syndrome, caused by *TBX5* mutations, where, with a different phenotype, the left side is also more affected (Mori and Bruneau, 2004). The basis for this left ‘sensitivity’ is unknown and the *Sox3* null mutation therefore represents a good model to study such symmetry-regulating mechanisms.

SOX3 and FGF signalling in pharyngeal arch development

Relatively few mutations show specific PA2 defects in mice. Among them, embryos homozygous for a hypomorphic mutation in *Fgfr1* ($Fgfr1^{n7/n7}$) show a PA2 phenotype strikingly similar to that described here for $Sox3^{\Delta gfp}$ (Trokovic et al., 2003; Trokovic et al., 2005). The expression of pouch markers becomes expanded across the remaining PA2 proximal domain in both mutants. Although *Fgfr1* is widely expressed in the pharyngeal region, Trokovic et al. (Trokovic et al., 2005) observed that *Fgf3* and *Fgf15* expression were lost specifically in the pharyngeal ectoderm of $Fgfr1^{n7/n7}$ embryos early during pharyngeal development (at 8 ss) and proposed that defects in the ectoderm are involved in abnormal pharyngeal morphogenesis. Embryos carrying a hypomorphic mutation in *Fgf8* also display hypoplastic pharyngeal arches in addition to several other abnormalities (Abu-Issa et al., 2002; Frank et al., 2002).

We were able to demonstrate a strong genetic interaction between *Sox3* and *Fgfr1*; however, we could not find any evidence for a linear relationship between the two genes or between *Sox3* and genes downstream of FGF signalling, such as *Sprouty-1*. This strongly

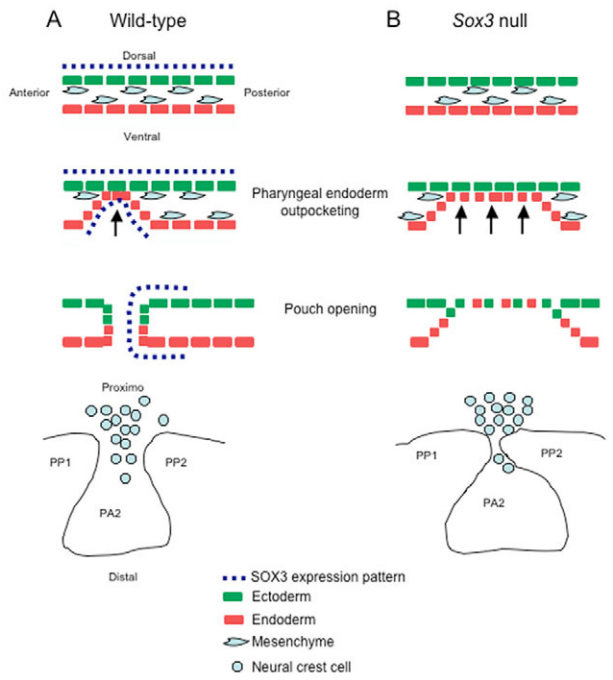

Fig. 9. Model illustrating the origin of the *Sox3* null PA2 phenotype. The position of future PP1 is determined by a focalised endodermal outpocketing at 8.0-8.5 dpc (**A**). Studies in urochordates (Manni et al., 2002) have shown that ectodermal and endodermal cell interdigitations then result in the opening of the pouch, surrounded by a newly formed epithelium, the pouch margin. At this stage SOX3 is restricted to the posterior pouch margin and ncc are migrating in PA2. In the absence of *Sox3* (**B**), the endoderm contacts the ectoderm over a much wider region, resulting in the formation of an enlarged pouch when the perforation occurs, and also an enlarged pouch margin. As a consequence, ncc migration is impaired.

suggests that SOX3 and FGF signalling act in parallel events during pharyngeal development. For example, one could be involved in identity/maintenance of the arch domain whereas the other would be more specifically required for pouch morphogenesis. As these two events are inter-dependent for PA2 morphogenesis, defects would be more severe in double mutants. Alternatively, the parallel pathways could eventually converge on a common target. Identification of genes regulated by SOXB1 factors in the pharyngeal region will further clarify their role.

In conclusion, we have shown that SOXB1 proteins are necessary during craniofacial development and that they act in connection with FGF signalling. The cellular origin of the defects strengthens the importance of the pharyngeal region for craniofacial development and gives new insight into pharyngeal pouch formation and the emergence of the arches during segmentation. Finally, these studies reveal how an early and relatively subtle defect affecting cellular properties leads to substantial consequences for craniofacial morphogenesis.

We wish to thank A. Graham (Kings College London), R. Krumlauf (Stowers Institute, Kansas City), P. Burgoyne, A. Matheu and A. Gould (NIMR), J. Partanen (University of Helsinki), Silvia Brunelli (San Raffaele Institute, Milan) and members of the lab for helpful discussions. We also thank J. Partanen and N. Trokovic for providing *Fgfr1* hypomorphic mice, and J. Collins for excellent technical assistance, W. Hatton for assistance with histology and P. Mealyer for taking care of the mouse colony. This work was supported by the MRC and by a Marie Curie Postdoctoral Fellowship to K.R.

References

Abu-Issa, R., Smyth, G., Smoak, I., Yamamura, K. and Meyers, E. N. (2002). Fgf8 is required for pharyngeal arch and cardiovascular development in the mouse. *Development* **129**, 4613-4625.

Arnold, J. S., Werling, U., Braunstein, E. M., Liao, J., Nowotschin, S., Edelmann, W., Hebert, J. M. and Morrow, B. E. (2006). Inactivation of Tbx1 in the pharyngeal endoderm results in 22q11DS malformations. *Development* **133**, 977-987.

Avilion, A. A., Bell, D. M. and Lovell-Badge, R. (2000). Micro-capillary tube in situ hybridisation: a novel method for processing small individual samples. *Genesis* **27**, 76-80.

Avilion, A. A., Nicolis, S. K., Pevny, L. H., Perez, L., Vivian, N. and Lovell-Badge, R. (2003). Multipotent cell lineages in early mouse development depend on SOX2 function. *Genes Dev.* **17**, 126-140.

Baker, C. V. and Bronner-Fraser, M. (2001). Vertebrate cranial placodes I. Embryonic induction. *Dev. Biol.* **232**, 1-61.

Bowl, M. R., Nesbit, M. A., Harding, B., Levy, E., Jefferson, A., Volpi, E., Rizzoti, K., Lovell-Badge, R., Schlessinger, D., Whyte, M. P. et al. (2005). An interstitial deletion-insertion involving chromosomes 2p25.3 and Xq27.1, near SOX3, causes X-linked recessive hypoparathyroidism. *J. Clin. Invest.* **115**, 2822-2831.

Brown, C. B., Wenning, J. M., Lu, M. M., Epstein, D. J., Meyers, E. N. and Epstein, J. A. (2004). Cre-mediated excision of Fgf8 in the Tbx1 expression domain reveals a critical role for Fgf8 in cardiovascular development in the mouse. *Dev. Biol.* **267**, 190-202.

Bulfone, A., Kim, H. J., Puelles, L., Porteus, M. H., Grippo, J. F. and Rubenstein, J. L. (1993). The mouse Dlx-2 (Tes-1) gene is expressed in spatially restricted domains of the forebrain, face and limbs in midgestation mouse embryos. *Mech. Dev.* **40**, 129-140.

Collignon, J., Sockanathan, S., Hacker, A., Cohen-Tannoudji, M., Norris, D., Rastan, S., Stevanovic, M., Goodfellow, P. N. and Lovell-Badge, R. (1996). A comparison of the properties of Sox-3 with Sry and two related genes, Sox-1 and Sox-2. *Development* **122**, 509-520.

Danielian, P. S., Muccino, D., Rowitch, D. H., Michael, S. K. and McMahon, A. P. (1998). Modification of gene activity in mouse embryos in utero by a tamoxifen-inducible form of Cre recombinase. *Curr. Biol.* **8**, 1323-1326.

Frank, D. U., Fotheringham, L. K., Brewer, J. A., Muglia, L. J., Tristani-Firouzi, M., Capecchi, M. R. and Moon, A. M. (2002). An Fgf8 mouse mutant phenocopies human 22q11 deletion syndrome. *Development* **129**, 4591-4603.

Gavalas, A., Trainor, P., Ariza-McNaughton, L. and Krumlauf, R. (2001). Synergy between Hoxa1 and Hoxb1: the relationship between arch patterning and the generation of cranial neural crest. *Development* **128**, 3017-3027.

Graham, A. and Smith, A. (2001). Patterning the pharyngeal arches. *BioEssays* **23**, 54-61.

Graham, A., Begbie, J. and McGonnell, I. (2004). Significance of the cranial neural crest. *Dev. Dyn.* **229**, 5-13.

Hebert, J. M. and McConnell, S. K. (2000). Targeting of cre to the Foxg1 (BF-1) locus mediates loxP recombination in the telencephalon and other developing head structures. *Dev. Biol.* **222**, 296-306.

Jerome, L. A. and Papaioannou, V. E. (2001). DiGeorge syndrome phenotype in mice mutant for the T-box gene, Tbx1. *Nat. Genet.* **27**, 286-291.

Laumonnier, F., Ronce, N., Hamel, B. C., Thomas, P., Lespinasse, J., Raynaud, M., Paringaux, C., Van Bokhoven, H., Kalscheuer, V., Fryns, J. P. et al. (2002). Transcription factor SOX3 is involved in X-linked mental retardation with growth hormone deficiency. *Am. J. Hum. Genet.* **71**, 1450-1455.

Mallo, M. (2001). Formation of the middle ear: recent progress on the developmental and molecular mechanisms. *Dev. Biol.* **231**, 410-419.

Manni, L., Nancy, J. L., Zaniolo, G. and Burighel, P. (2002). Cell reorganisation during epithelial fusion and perforation: the case of the ascidian branchial fissures. *Dev. Dyn.* **224**, 303-313.

Mori, A. D. and Bruneau, B. G. (2004). TBX5 mutations and congenital heart disease: Holt-Oram syndrome revealed. *Curr. Opin. Cardiol.* **19**, 211-215.

O'Gorman, S. (2005). Second branchial arch lineages of the middle ear of wild-type and Hoxa2 mutant mice. *Dev. Dyn.* **234**, 124-131.

Quinlan, R., Martin, P. and Graham, A. (2004). The role of actin cables in directing the morphogenesis of the pharyngeal pouches. *Development* **131**, 593-599.

Raverot, G., Weiss, J., Park, S. Y., Hurley, L. and Jameson, J. L. (2005). Sox3 expression in undifferentiated spermatogonia is required for the progression of spermatogenesis. *Dev. Biol.* **283**, 215-225.

Rizzoti, K., Brunelli, S., Carmignac, D., Thomas, P. Q., Robinson, I. C. and Lovell-Badge, R. (2004). SOX3 is required during the formation of the hypothalamo-pituitary axis. *Nat. Genet.* **36**, 247-255.

Robson, H., Siebler, T., Shalet, S. M. and Williams, G. R. (2002). Interactions between GH, IGF-I, glucocorticoids, and thyroid hormones during skeletal growth. *Pediatr. Res.* **52**, 137-147.

Serbedzija, G. N., Bronner-Fraser, M. and Fraser, S. E. (1992). Vital dye analysis

of cranial neural crest cell migration in the mouse embryo. *Development* **116**, 297-307.
Trokovic, N., Trokovic, R., Mai, P. and Partanen, J. (2003). Fgfr1 regulates patterning of the pharyngeal region. *Genes Dev.* **17**, 141-153.
Trokovic, N., Trokovic, R. and Partanen, J. (2005). Fibroblast growth factor signalling and regional specification of the pharyngeal ectoderm. *Int. J. Dev. Biol.* **49**, 797-805.
Veitch, E., Begbie, J., Schilling, T. F., Smith, M. M. and Graham, A. (1999). Pharyngeal arch patterning in the absence of neural crest. *Curr. Biol.* **9**, 1481-1484.
Vitelli, F., Taddei, I., Morishima, M., Meyers, E. N., Lindsay, E. A. and Baldini, A. (2002). A genetic link between Tbx1 and fibroblast growth factor signaling. *Development* **129**, 4605-4611.
Wegner, M. and Stolt, C. C. (2005). From stem cells to neurons and glia: a Soxist's view of neural development. *Trends Neurosci.* **28**, 583-588.
Weiss, J., Meeks, J. J., Hurley, L., Raverot, G., Frassetto, A. and Jameson, J. L. (2003). Sox3 is required for gonadal function, but not sex determination, in males and females. *Mol. Cell. Biol.* **23**, 8084-8091.
Wood, H. B. and Episkopou, V. (1999). Comparative expression of the mouse Sox1, Sox2 and Sox3 genes from pre-gastrulation to early somite stages. *Mech. Dev.* **86**, 197-201.
Wurdak, H., Ittner, L. M. and Sommer, L. (2006). DiGeorge syndrome and pharyngeal apparatus development. *BioEssays* **28**, 1078-1086.
Zucker, R. M., Hunter, E. S., 3rd and Rogers, J. M. (1999). Apoptosis and morphology in mouse embryos by confocal laser scanning microscopy. *Methods* **18**, 473-480.